Brannerite-Type Vanadium−Molybdenum Oxide LiVMoO$_6$ as a Promising Anode Material for Lithium-Ion Batteries with High Capacity and Rate Capability

Nan Chen,[†,‡] Chunzhong Wang,[†,‡] Fang Hu,[§] Xiaofei Bie,[†,∥] Yingjin Wei,[†] Gang Chen,[†,‡] and Fei Du*[,†]

[†]Key Laboratory of Physics and Technology for Advanced Batteries (Ministry of Education), College of Physics and [‡]State Key Laboratory of Superhard Materials, Jilin University, Changchun 130012, PR China

[§]School of Materials Science and Engineering, Shenyang University of Technology, Shenyang 110870, PR China

[∥]Elements Strategy Initiative for Catalysts and Batteries, Kyoto University, Kyoto 615-8520, Japan

ABSTRACT: Brannerite-type vanadium−molybdenum oxide LiV-MoO$_6$ is prepared by a facile liquid-phase method, and its electrochemical properties as anode of lithium-ion batteries are comprehensively studied by means of galvanostatic charge−discharge profiles, rate performance, and cyclic voltammetry. In the working voltage between 3.0 and 0.01 V, LiVMoO$_6$ delivers a high reversible capacity of more than 900 mAh g^{-1} at the current density of 100 mA g^{-1} and a superior rate capability with discharge capacity of ca. 584 and 285 mAh g^{-1} under the high current densities of 2 and 5 A g^{-1}, respectively. Moreover, ex situ X-ray diffraction and X-ray photoelectron spectroscopy are utilized to examine the phase evolution and valence changes during the first lithiated process. A small amount of inserted Li$^+$ induces a decomposition of LiVMoO$_6$

into Li$_2$Mo$_2$O$_7$ and V$_2$O$_5$, which play the host during further lithiated processes. When being discharged to 0.01 V, most V^{5+} change into V^{3+}/V^{2+}, suggesting intercalation/deintercalation processes, whereas Mo^{6+} are reduced into a metallic state on the basis of the conversion reaction. The insights obtained from this study will benefit the design of novel anode materials for lithium-ion batteries.

KEYWORDS: lithium-ion batteries, anode materials, vanadium−molybdenum oxide, electrochemical properties, lithiated mechanism
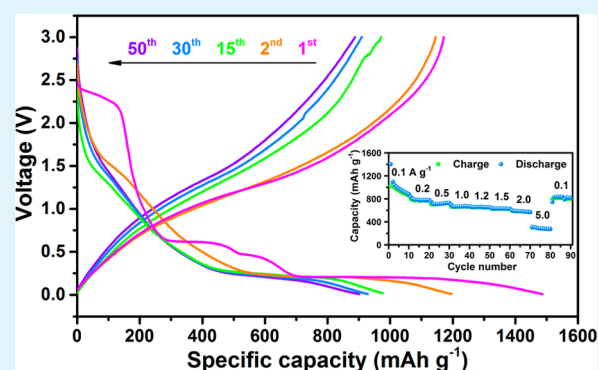
INTRODUCTION

With the rapid development of portable electronic devices, especially electric vehicles (EVs) and hybrid electric vehicles (HEVs), the great demands for advanced lithium-ion batteries (LIBs) triggered the extensive studies on the novel electrode materials with high energy and power densities.[1−4] During recent decades, transition metal oxides (TMOs),[5−11] as one of the potential alternative anode materials of LIBs, have attracted significant interest owing to their low cost, hypotoxicity, and natural abundance. TMOs, on the basis of the conversion mechanism, show much better Li-ion storage capability than that of graphite anodes in terms of high reversible capacity, remarkable rate performance, and other properties. Nevertheless, these compounds still suffer from some disadvantages such as low electrical conductivity and poor durability because of the drastic volume change during Li$^+$ intercalation and deintercalation processes.

Until now, many strategies have been proposed to tackle the above-mentioned issues of TMO anodes. One effective approach is to fabricate their binary and ternary derivatives because of the diverse functionalities integrated in one single object. Molybdenum-based oxides can deliver high capacity owing to the great ability of Mo to exist in several oxidation

states ranging from +6 to 0 when being discharged to near 0 V vs Li/Li$^+$. Encouragingly, their binary compounds, such as MeMoO$_4$ (Me = Co, Zn, Mn, Ni, etc.),[12−16] also show high reversible capacity, good rate capability, and cycle stability. Their electrochemical activities related to the complex chemical compositions and synergistic effects contribute to exceptional performance. Also, these compounds exhibit high electrical conductivity compared with that of the simple TMOs owing to the relatively low activation energy for electron transfer among cations. For example, CoMoO$_4$ submicrometer particles show a stable capacity of nearly 1000 mAh g^{-1} between 3.0 and 0.005 V over 40 cycles.[12] The nanocomposite between CoMoO$_4$ nanoparticles and reduced graphene oxide delivers an excellent cycle stability over 600 cycles with a high specific capacity of 740 mAh g^{-1}.[17]

LiMoVO$_6$ crystallizes in the ThTi$_2$O$_6$-type brannerite structure, where a quasi-2D structure is built up by the edge-sharing VO$_6$ and MoO$_6$ octahedra along b axis. Lithium ions are situated between the anionic sheets in LiO$_6$ octahedral

sites.[18−20] Its electrochemical properties were once studied in different working voltages: Between 1.8 and 3.6 V, rodlike LiVMoO$_6$ nanocrystals delivered a stable capacity of 166 mAh g^{-1} at a current density of 200 mA g^{-1} over 100 cycles.[21] Though the reversible capacity is comparable with that of commercial LiCoO$_2$, the low average working voltage at around 2.3 V definitely induces a low-energy density when utilized as the cathode in a full cell. When lowering the working potential to nearly 0 V, a high discharge capacity of nearly 1200 mAh g^{-1} was achieved. A large capacity loss of more than 600 mAh g^{-1}, however, was found, and the cycle stability was also unsatisfactory.[22,23]

In this work, a facile liquid-phase method employed to prepare brannerite-type LiVMoO$_6$ and the electrochemical properties between 3.0 and 0.01 V are examined by charge−discharge tests, rate capability, and cyclic voltammetry (CV). Additionally, the structural evolution and valence changes of the first lithiated process are studied using ex situ X-ray diffraction (XRD) and X-ray photoelectron spectroscopy (XPS).

EXPERIMENTAL SECTION

Brannerite-type LiVMoO$_6$ was synthesized by a facile liquid-phase method. First, 0.0357 M (NH$_4$)$_6$Mo$_7$O$_{24}$·4H$_2$O, 0.5 M LiOH·H$_2$O, and 0.25 M NH$_4$VO$_3$ aqueous solution were prepared. Then, (NH$_4$)$_6$Mo$_7$O$_{24}$·4H$_2$O (40 mL) and LiOH·H$_2$O (20 mL) were added dropwise into the solution of NH$_4$VO$_3$ (40 mL) in sequence. After continuous magnetic stirring at 80 °C for 12 h, the dried precursor was ground in an agate mortar and pressed into a pellet. After sintering in air at 550 °C for 6 h with an intermediate grinding, the resulting yellow LiVMoO$_6$ powder could be obtained. Powder XRD pattern was recorded in the 2θ range 10−55° at a scanning rate of 2°/min using a Bruker D8 with diffractometer a Cu Kα source. The particle sizes and morphologies were observed by Hitachi SU8020 type scanning electron microscopy (SEM). The microstructure was studied by a FEI Tecnai G2 type transmission electron microscopy (TEM). XPS was carried out on a VG scientific ESCALAB-250 spectrometer. The binding energy was corrected using the C 1s peak at 284.6 eV. To obtain detailed information on the chemical state of the transition metal ions in the materials bulk, all the samples were sputtered by Ar-ion beam for 90 s and then subjected to XPS analysis.

Electrochemical experiments were carried out using 2032-type coin cells. A typical electrode was composed of LiVMoO$_6$ active material (70 wt %), carbon black conductive additive (20 wt %), carboxy methyl cellulose (CMC 5 wt %), and styrene butadiene rubber (SBR, 5 wt %) dissolved in deionized water. The slurry mixture was pasted on a copper foil, followed by drying at 120 °C for 12 h in a vacuum oven. Each electrode was 8 × 8 mm^2 in size. The cathode and anode electrodes were separated by Celgard 2320 membrane. The electrolyte was a 1 M lithium hexafluorophosphate (LiPF$_6$) dissolved in ethylene carbonate (EC), dimethyl carbonate (DMC), and ethyl methyl carbonate (EMC) with EC: DMC: EMC = 1:1:8 by volume. Galvanostatic charge−discharge cycling was performed on a Land-2001A (Wuhan, China) automatic battery tester. CV was recorded on a VSP multichannel potentiostatic−galvanostatic system (Biologic, France) at a scanning rate of 0.1 mV s^{-1}.

RESULTS AND DISCUSSION

Figure 1 shows the XRD pattern of pristine LiVMoO$_6$. All the diffraction peaks can be indexed on the basis of the monoclinic symmetry (space group C2/m) with no trace of impurity phases. The lattice constants are calculated to be a = 9.3643 Å, b = 3.6574 Å, c = 6.6532 Å, and β = 111.660°, which are consistent with the previous reports.[18] As displayed in Figure 2a, the SEM image exhibits the blocklike morphology and clean surface. The particle sizes are not uniform, ranging from 0.1 to
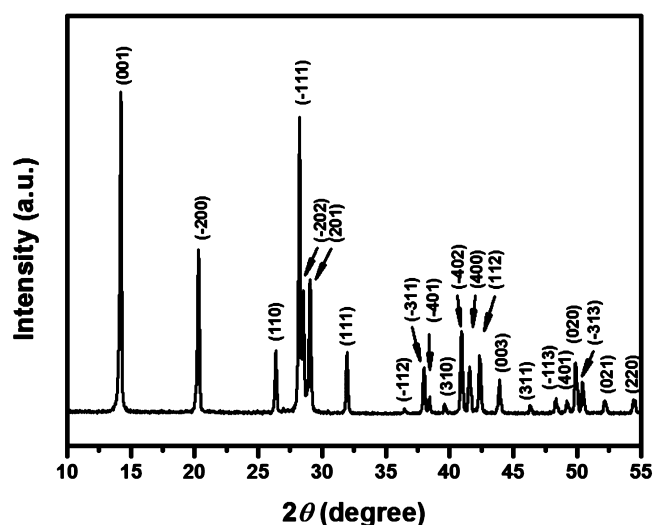

Figure 1. X-ray diffraction pattern of the pristine LiVMoO$_6$.

2 μm. The corresponding SAED pattern based on one small particle confirms the single-phase nature of LiVMoO$_6$ sample. To identify the distribution of different ions, element mapping for the pristine sample is provided in Figure 3, which clearly shows that V, Mo, and O are uniformly distributed in the material.

Galvanostatic charge−discharge profiles for LiVMoO$_6$ are examined in the voltage range between 3.0 and 0.01 V under the current density of 100 mA g^{-1}, as presented in Figure 4a. As can be seen, multistep electrochemical reactions are clearly observed in the first discharge process. At ca. 2.3 V, a working plateau appears in the first discharge curve but disappears in the subsequent cycles, which is related to the irreversible structural decomposition of LiVMoO$_6$. This phase transition is also confirmed by the following ex situ XRD studies. With decreasing working potentials, another two small plateaus at around 0.6 and 0.45 V are found. Because no structural transition can be detected below 1.0 V, the manifested plateaus should be ascribed to the further reduction of V^{5+}/Mo^{6+} into their low valence states and formation of a solid electrolyte interface (SEI) film because of the decomposition of the electrolyte.[24,25] At around 0.2 V, a long, flat potential region corresponding to nearly 800 mAh g^{-1} is realized in the first discharge profile and is maintained even after 50 cycles, suggesting a highly reversible Li$^+$-inserted/extracted processes. The first discharge curve differs from the successive scans, and charge/discharge profiles are analogous to each other by the third cycle, which indicates that the irreversible structural transition finishes after the first two cycles and a weak polarization in the proposed cell. Moreover, the electrode demonstrates good cycle stability, as exhibited in Figure 4. After the gradual activation of some cell components for several cycles, the stable specific capacity of 910 mAh g^{-1} is achieved with the Coulombic efficiency above 98%. However, the initial capacity loss of nearly 300 mAh g^{-1} may be caused by the formation of SEI film or the poor electrical/ionic conductivity of the resultant.[26−31] Also, the irreversible structural transition from LiVMoO$_6$ into Li$_2$Mo$_2$O$_7$ and V$_2$O$_5$ during the first discharge process (see ex situ XRD discussion) can induce the large capacity loss.

Besides the high capacity and good cycle stability, LiVMoO$_6$ also exhibits a superior rate capability, as displayed in Figure 5.

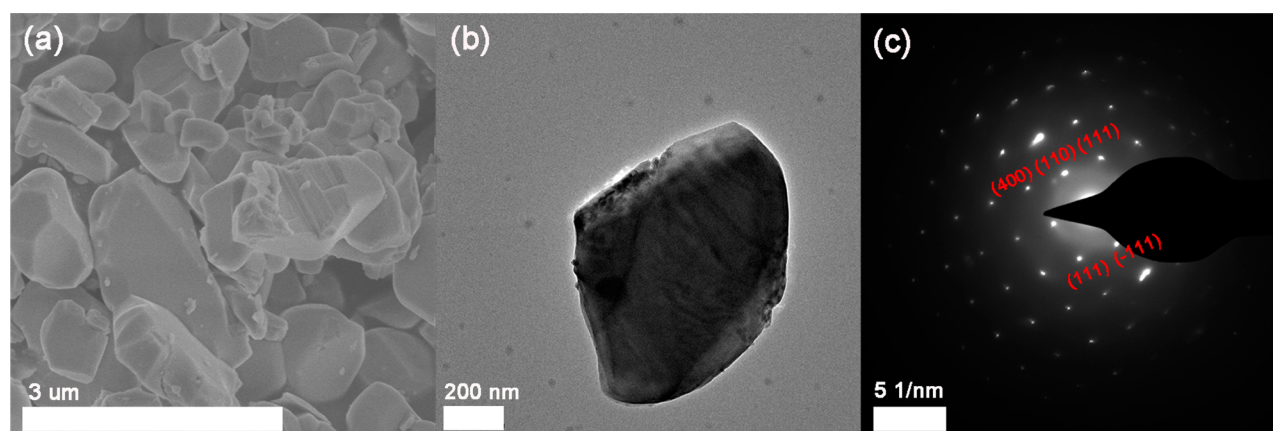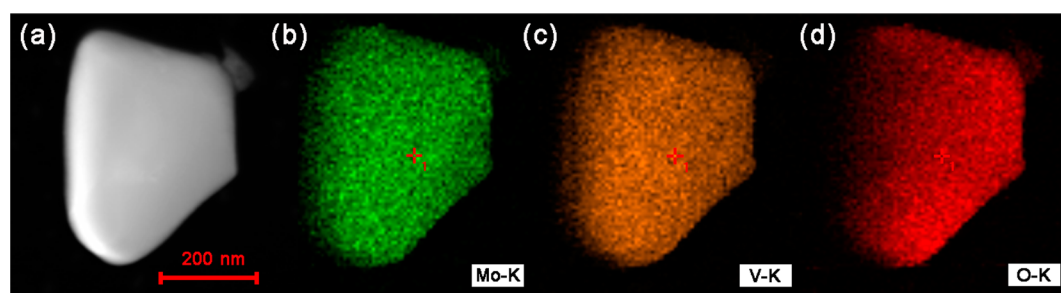**Figure 2.** (a) SEM image, (b) TEM image, and (c) SAED pattern of LiVMoO$_6$.

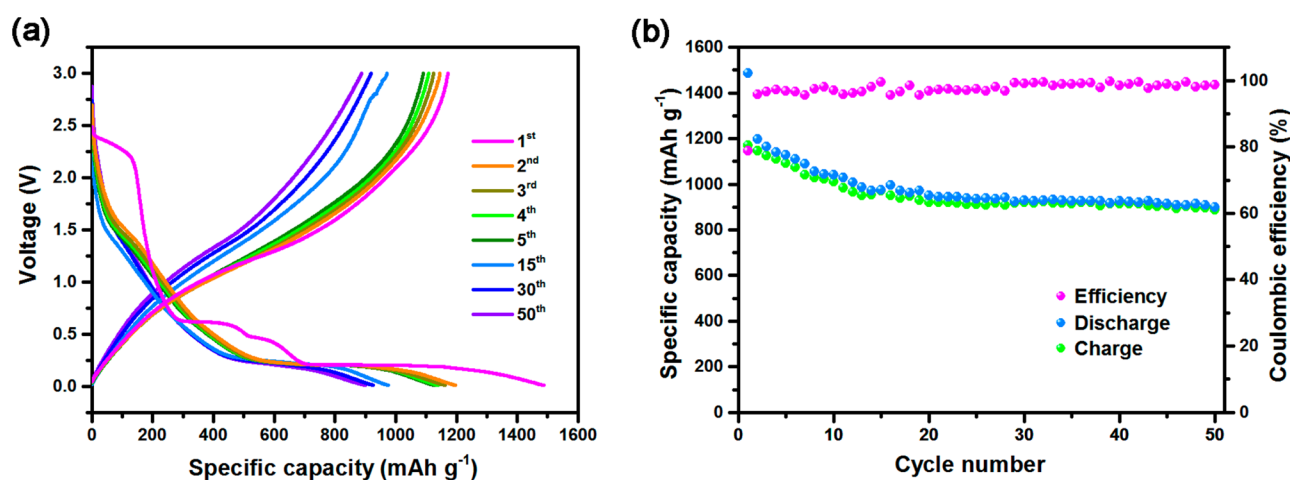**Figure 3.** (a) HAADF-STEM image and mappings of the (b) Mo, (c) V, and (d) O elements for LiVMoO$_6$.

Figure 4. (a) Galvanostatic charge−discharge curves between 3.0 and 0.01 V at a constant current density of 100 mA g^{-1}. (b) Cycle performance and Coulombic efficiency for 50 cycles of LiVMoO$_6$.

The electrode delivers reversible capacities of 780, 730, 674, 665, 634, and 584 mAh g^{-1} as the current densities increasing from 0.2 to 0.5, 1, 1.2, 1.5, and 2 A g^{-1}, respectively. Even under the high current density of 5 A g^{-1}, LiVMoO$_6$ shows a reversible capacity of 285 mAh g^{-1}, much higher than that of the commercial graphite anode and even comparable with that of the widely studied TMOs anode.[8,26,32−34] Furthermore, when the current density returns to 0.1 A g^{-1} after 80 cycles, the stable capacity reaches 820 mAh g^{-1}, in contrast to the capacity degradation for the first 10 cycles caused by the gradual activation of the cell. As a result, the LiVMoO$_6$ electrode exhibits the overall electrochemical performances in terms of high reversible capacity, excellent cycle stability, and

rate capability among the binary or ternary TMOs anode materials.[35−37]

To understand the electrochemical redox processes of LiVMoO$_6$, the CV profiles for five cycles (Figure 6) are recorded at a scan rate of 0.1 mV s^{-1} vs Li/Li$^+$ between 3.0 and 0.01 V. In the first cathodic scan, four intensive reduction peaks are located at nearly 2.18, 0.47, 0.4, and 0.02 V, matching well to the working plateaus in the first discharge profile. The large particle size of pristine LiVMoO$_6$ and inadequate contact with electrolyte result in the incomplete electrochemical reaction manifested as two broad peaks at 2.28 and 0.57 V with less intensity in the second cathodic scan. In contrast, the first anodic scan shows various oxidation peaks related to the
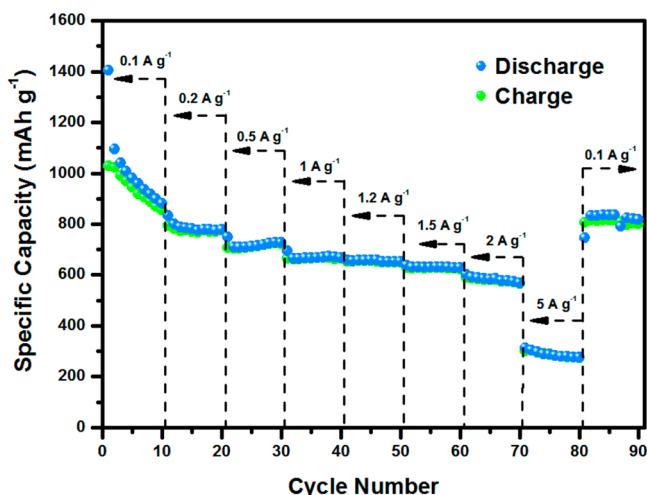
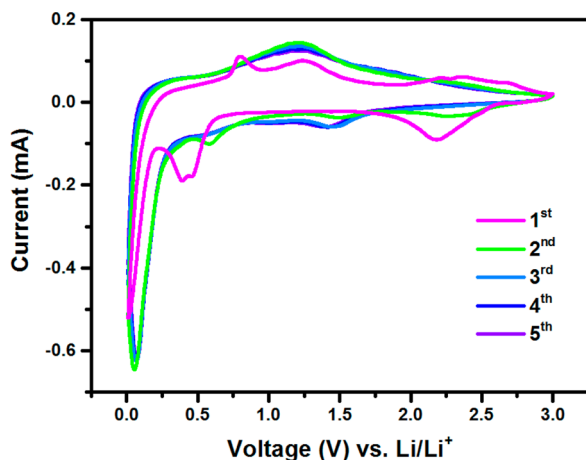**Figure 5.** Rate performance of $LiVMoO_6$ in the voltage region of 3.0–0.01 V at various current densities.

**Figure 6.** Cyclic voltammograms of $LiVMoO_6$ electrode at a scan rate of 0.1 mV s^{-1}.

multiple steps of a Li$^+$-extraction process attributable to the great ability of Mo and V to exist in several oxidation states, ranging from +6 to 0 for Mo and from +5 to +2 for V. From the third scan onward, nearly all the CV profiles are superimposed upon each other, indicative of highly reversible Li$^+$-insertion/extraction processes. In addition, the cathodic scans after the third scan show two reduction peaks at 1.4 and 0.06 V, which can be attributed to the lithiated process in the V-based oxides and reduction reaction of Mo from +6 to 0,[38,39] respectively, whereas only one oxidation peak at 1.2 V can be detected because of the overlap of oxidation peaks from V^{5+} into V^{2+} and Mo^0 into Mo^{6+}. Similar lithiated/delithiated processes have also been proposed in various oxides, such as $Co_3V_2O_8$,[38] $CoMoO_4$,[12] ZnV_2O_4,[40,41] and Li_2MoO_4,[42] among others.

Ex situ XPS (Figure 7) and XRD (Figure 8) of the electrodes at different discharge depths are conducted to further clarify the electrochemical processes during the first lithiated cycle. As shown in Figure 7a,b, two split peaks located at 523.9 and 516.7 eV can be assigned as V^{5+} 2p$_{1/2}$ and 2p$_{3/2}$,[43,44] respectively, whereas the peaks at 235.8 and 232.7 eV are assigned as Mo^{6+} 2p$_{3/2}$ and 2p$_{5/2}$.[45,46] Hence, both vanadium and molybdenum are in their highest oxidized states in $LiVMoO_6$. When being

discharged to 0.4 V (Figure 7c), most V^{5+} are reduced into V^{4+} and V^{3+}. Meanwhile, the Mo 3d spectrum can be fitted to two components, Mo^{4+} and Mo^{6+}, which is consistent with the reduction steps for molybdenum oxides. When the electrode discharged to 0.01 V, V^{3+} and V^{2+} are in the majority though a small amount of V^{4+} and V^{5+} remain because of the incomplete electrochemical reaction, whereas the existence of Mo^0, characteristic of two split peaks at 231.5 (Mo 3d$_{5/2}$) and 228.3 eV (Mo 3d$_{3/2}$),[45] strongly suggests that most molybdenum is in the metallic state.
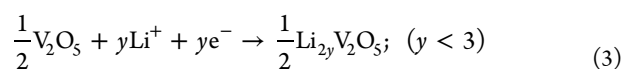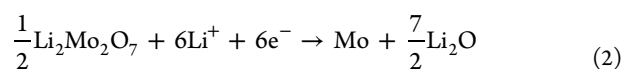
Furthermore, as presented in Figure 8, it can be seen that an abrupt structural transition takes place as voltage decreases from the open-circuit voltage (OCV) to 2.4 V. Accordingly, an extremely low specific capacity of less than 20 mAh g^{-1}, corresponding to nearly 0.2 Li$^+$ insertion, is delivered. Such a small amount of Li$^+$ insertion triggers the complete phase decomposition possibly owing to the bad structural tolerance of $LiVMoO_6$. After careful indexing, the diffraction data at 2.4 V can be considered to show the coexistence of two phases of $Li_2Mo_2O_7$ (Powder Diffraction File (PDF) no. 24−0641, International Centre for Diffraction Data (ICDD), 1971) and V_2O_5 (PDF no. 01−0359, ICDD, 1928). The two phases remain unchanged as the voltage decreases to 0.4 V, though some peaks shift can be observed. Such a shift suggests that $Li_2Mo_2O_7$ and V_2O_5 are likely to play the host and further accommodate Li$^+$. Note that any diffraction peaks of Mo or vanadium oxides can hardly be detected when being discharged to 0.01 V. This phenomenon can be attributed to the nanoparticle nature of electrochemically formed species inserted into the amorphous Li_2O matrix, which has been observed in the $ZnMn_2O_4$[47] and $CoMoO_4$[12] anode materials.

On the basis of the experimental results of this study, a possible lithiated mechanism of $LiVMoO_6$ material in the first discharged process is proposed as eq 1 to 3. The appearance of reduced V^{2+}/V^{3+} at the end of the first discharge stage suggests an intercalation/deintercalation processes for vanadium oxides, whereas Mo^{6+} is likely to be reduced into its metallic state according to the conversion mechanism. Furthermore, the high specific capacity of $LiVMoO_6$ of nearly 900 mAh g^{-1} is consistent with its theoretical expected value that is based on the reversible redox of vanadium from +5 to +2/+3 and molybdenum from +6 to 0. It is interesting to note that the $LiVMoO_6$ electrode exhibits much higher capacities and better cyclability than vanadium oxides compounds such as ZnV_2O_4,[40] $Zn_3V_2O_8$[24] and ZnV_2O_6,[48] owing to the great ability of Mo to exist in several oxidation states and the synergistic effects of different electrochemical mechanisms. When molybdenum oxides experience lithiated/delithiated processes, the vanadium oxides can act as the matrix to alleviate the effect of volume expansion during most Li$^+$ insertion. Thanks to the superior cycle stability and minor volume expansion of intercalation-type anodes, preparation of the binary or ternary compounds on the basis of the intercalation/deintercalation and alloying/dealloying processes, the intercalation/deintercalation mechanism and conversion reactions, or even all three might be an effective approach to achieve novel anode materials with high energy and power densities.

$$LiVMoO_6 + xLi + xe^-$$
$$\rightarrow \frac{1}{2}Li_2Mo_2O_7 + \frac{1}{2}V_2O_5; \ (x < 0.2) \tag{1}$$
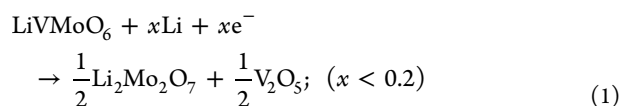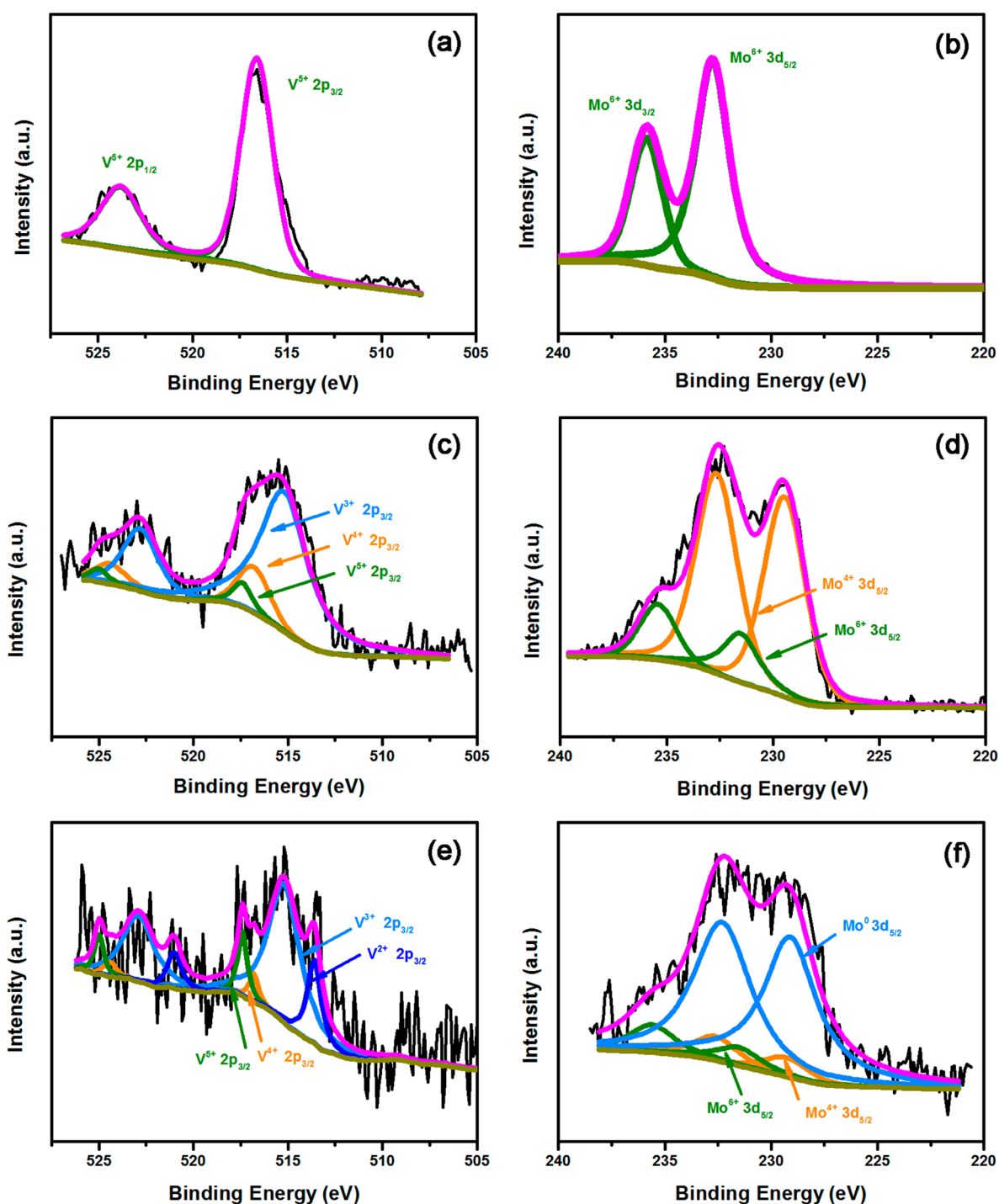
Figure 7. XPS spectra of V 2p and Mo 3d, respectively, for (a and b) pristine LiVMoO$_6$, (c and d) reduced electrode obtained at 0.4 V, and (e and f) fully discharged electrode obtained at 0.01 V.

$$\frac{1}{2}\text{Li}_2\text{Mo}_2\text{O}_7 + 6\text{Li}^+ + 6e^- \rightarrow \text{Mo} + \frac{7}{2}\text{Li}_2\text{O} \qquad (2)$$

$$\frac{1}{2}\text{V}_2\text{O}_5 + y\text{Li}^+ + ye^- \rightarrow \frac{1}{2}\text{Li}_{2y}\text{V}_2\text{O}_5; \quad (y < 3) \qquad (3)$$

■ CONCLUSIONS

Brannerite-type LiVMoO$_6$ is synthesized by a facile liquid-phase method. The electrode delivers a high reversible capacity of more than 900 mAh g^{-1} at a current density of 100 mA g^{-1}

between 3.0 and 0.01 V. Also, it exhibits a superior rate capability with discharge capacity of ca. 584 and 285 mAh g^{-1} under the high current densities of 2 and 5 A g^{-1}, respectively. Ex situ XRD and XPS during the first lithiated process demonstrate an obvious structural transition from LiVMoO$_6$ into Li$_2$Mo$_2$O$_7$ and V$_2$O$_5$ when being discharged to 2.4 V, which will play the host for further lithiated processes. When being discharged to 0.01 V, most V^{5+} are changed into V^{3+}/V^{2+}, whereas the existence of Mo^0 indicates that Mo^{6+} are reduced into the metallic state on the basis of the conversion reaction. Thanks to the high reversible capacity and excellent rate
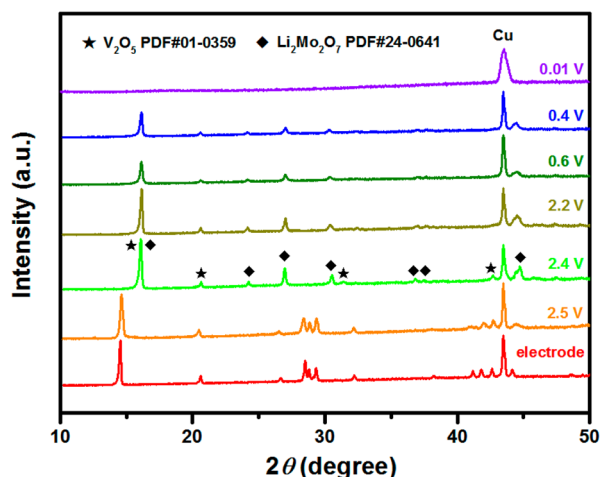
Figure 8. Ex situ XRD patterns of the $LiVMoO_6$ electrode at different lithiated stages during the first discharge process.

performance, $LiVMoO_6$ is considered a promising anode material for LIBs.

■ AUTHOR INFORMATION

Corresponding Author
*E-mail: dufei@jlu.edu.cn.

Notes
The authors declare no competing financial interest.

■ ACKNOWLEDGMENTS

■ REFERENCES

(1) Armand, M.; Tarascon, J. M. Building Better Batteries. *Nature* **2008**, *451*, 652−657.

(2) Tarascon, J. M.; Armand, M. Issues and Challenges Facing Rechargeable Lithium Batteries. *Nature* **2001**, *414*, 359−367.

(3) Huang, X. L.; Zhao, X.; Wang, Z. L.; Wang, L. M.; Zhang, X. B. Facile and Controllable One-Pot Synthesis of An ordered nanostructure of $Co(OH)_2$ Nanosheets and Their Modification by Oxidation for High-Performance Lithium-Ion Batteries. *J. Mater. Chem.* **2012**, *22*, 3764−3769.

(4) Huang, X. L.; Chai, J.; Jiang, T.; Wei, Y. J.; Chen, G.; Liu, W. Q.; Han, D. X.; Niu, L.; Wang, L. M.; Zhang, X. B. Self-Assembled Large-Area $Co(OH)_2$ Nanosheets/Ionic Liquid Modified Graphene Heterostructures toward Enhanced Energy Storage. *J. Mater. Chem.* **2012**, *22*, 3404−3410.

(5) Tarascon, J.-M.; Poizot, P.; Laruelle, S.; Grugeon, S.; Dupont, L. Nano-Sized Transition-Metal Oxides as Negative-Electrode Materials for Lithium-Ion Batteries. *Nature* **2000**, *407*, 496−499.

(6) Reddy, M. V.; Subba Rao, G. V.; Chowdari, B. V. Metal Oxides and Oxysalts as Anode Materials for Li Ion Batteries. *Chem. Rev.* **2013**, *113*, 5364−5457.

(7) Huang, Y.; Huang, X. L.; Lian, J. S.; Xu, D.; Wang, L. M.; Zhang, X. B. Self-Assembly of Ultrathin Porous NiO Nanosheets/Graphene Hierarchical Structure for High-Capacity and High-Rate Lithium Storage. *J. Mater. Chem.* **2012**, *22*, 2844−2847.

(8) Huang, X. L.; Wang, R. Z.; Xu, D.; Wang, Z. L.; Wang, H. G.; Xu, J. J.; Wu, Z.; Liu, Q. C.; Zhang, Y.; Zhang, X. B. Homogeneous CoO on Graphene for Binder-Free and Ultralong-Life Lithium Ion Batteries. *Adv. Funct. Mater.* **2013**, *23*, 4345−4353.

(9) Wang, H. G.; Ma, D. L.; Huang, X. L.; Huang, Y.; Zhang, X. B. General and Controllable Synthesis Strategy of Metal Oxide/TiO_2 Hierarchical Heterostructures with Improved Lithium-Ion Battery Performance. *Sci. Rep.* **2012**, *2*, 1−8.

(10) Su, P. P.; Liao, S. C.; Rong, F.; Wang, F. Q.; Chen, J.; Li, C.; Yang, Q. H. Enhanced Lithium Storage Capacity of Co_3O_4 Hexagonal Nanorings Derived from Co-Based Metal Organic Frameworks. *J. Mater. Chem. A* **2014**, *2*, 17408−17414.

(11) Hassan, M. F.; Guo, Z. P.; Chen, Z.; Liu, H. K. Carbon-Coated MoO_3 Nanobelts as Anode Materials for Lithium-Ion Batteries. *J. Power Sources* **2010**, *195*, 2372−2376.

(12) Cherian, C. T.; Reddy, M. V.; Haur, S. C.; Chowdari, B. V. Interconnected Network of $CoMoO_4$ Submicrometer Particles as High Capacity Anode Material for Lithium Ion Batteries. *ACS Appl. Mater. Interfaces* **2013**, *5*, 918−923.

(13) Cao, Y. J.; Li, W. Y.; Xu, K. B.; Zhang, Y. X.; Ji, T.; Zou, R. J.; Yang, J. M.; Qin, Z. Y.; Hu, J. Q. $MnMoO_4·4H_2O$ Nanoplates Grown on a Ni Foam Substrate for Excellent Electrochemical Properties. *J. Mater. Chem. A* **2014**, *2*, 20723−20728.

(14) Peng, C.; Gao, L.; Yang, S. W.; Sun, J. A General Precipitation Strategy for Large-Scale Synthesis of Molybdate Nanostructures. *Chem. Commun.* **2008**, 5601−5603.

(15) Young, A. P.; Schwartz, C. M. High-Pressure Synthesis of Molybdates with the Wolframite Structure. *Science* **1963**, *141*, 348−349.

(16) Leyzerovich, N. N.; Bramnik, K. G.; Buhrmester, T.; Ehrenberg, H.; Fuess, H. Electrochemical Intercalation of Lithium in Ternary Metal Molybdates $MMoO_4$ (M: Cu, Zn, Ni and Fe). *J. Power Sources* **2004**, *127*, 76−84.

(17) Yao, J.; Gong, Y.; Yang, S.; Xiao, P.; Zhang, Y.; Keyshar, K.; Ye, G.; Ozden, S.; Vajtai, R.; Ajayan, P. M. $CoMoO_4$ Nanoparticles Anchored on Reduced Graphene OxideNanocomposites as Anodes for Long-Life Lithium-Ion Batteries. *ACS Appl. Mater. Interfaces* **2014**, *6*, 20414−20422.

(18) Ezzine Yahmed, S.; Nasri, R.; Zid, M. F.; Driss, A. Lithium vanado(V)molybdate(VI), $Li[VMoO_6]$. *Acta Crystallogr., Sect. E: Struct. Rep. Online* **2013**, *69*, i57−i58.

(19) Cushing, B. L.; Kang, S. H.; Goodenough, J. B. Instability of Brannerite Cathode Materials upon Lithium Insertion. *Int. J. Inorg. Mater.* **2001**, *3*, 875−879.

(20) Amdouni, N.; Zarrouk, H.; Soulette, F.; Julien, C. M. Synthesis, Structure and Lithium Intercalation Reaction in $LiMoVO_6$ Brannerite-Type Materials. *J. Mater. Chem.* **2003**, *13*, 2374−2380.

(21) Zhou, L.; Liang, Y.; Hu, L.; Han, X.; Yi, Z.; Sun, J.; Yang, S. Much Improved Capacity and Cycling Performance of $LiVMoO_6$ Cathode for Lithium Ion Batteries. *J. Alloys Compd.* **2008**, *457*, 389−393.

(22) Liu, R. S.; Wang, C. Y.; Drozd, V. A.; Hu, S. F.; Sheu, H. S. A Novel Anode Material $LiVMoO_6$ for Rechargeable Lithium-Ion Batteries. *Electrochem. Solid-State Lett.* **2005**, *8*, A650−A653.

(23) Liang, Y.; Yang, S.; Yi, Z.; Li, M.; Sun, J.; Zhou, Y. Rheological Phase Synthesis and Electrochemical Performances of $LiVMoO_6$ as A High-Capacity Anode Material for Lithium Ion Batteries. *J. Mater. Sci.* **2005**, *40*, 5553−5555.

(24) Gan, L.-H.; Deng, D.; Zhang, Y.; Li, G.; Wang, X.; Jiang, L.; Wang, C.-R. $Zn_3V_2O_8$ Hexagon Nanosheets: A High-Performance Anode Material for Lithium-Ion Batteries. *J. Mater. Chem. A* **2014**, *2*, 2461−2466.

(25) Tao, T.; Glushenkov, A. M.; Zhang, C. F.; Zhang, H. Z.; Zhou, D.; Guo, Z. P.; Liu, H. K.; Chen, Q. Y.; Hu, H. P.; Chen, Y. MoO_3 Nanoparticles Dispersed Uniformly in Carbon Matrix: a High

Capacity Composite Anode for Li-Ion Batteries. *J. Mater. Chem.* **2011**, *21*, 9350−9355.

(26) Zhu, Y.; Guo, H.; Wu, Y.; Cao, C.; Tao, S.; Wu, Z. Surface-Enabled Superior Lithium Storage of High-Quality Ultrathin NiO Nanosheets. *J. Mater. Chem. A* **2014**, *2*, 7904−7911.

(27) Saadat, S.; Zhu, J. X.; Sim, D. H.; Hng, H. H.; Yazami, R.; Yan, Q. Y. Coaxial Fe_3O_4/CuO Hybrid Nanowires as Ultra Fast Charge/Discharge Lithium-Ion Battery Anodes. *J. Mater. Chem. A* **2013**, *1*, 8672−8678.

(28) Osiak, M.; Geaney, H.; Armstrong, E.; O'Dwyer, C. Structuring Materials for Lithium-Ion Batteries: Advancements in Nanomaterial Structure, Composition, and Defined Assembly on Cell Performance. *J. Mater. Chem. A* **2014**, *2*, 9433−9460.

(29) Li, S. Y.; Xie, W. H.; Wang, S. Y.; Jiang, X. Y.; Peng, S. L.; He, D. Y. Facile Synthesis of rGO/SnO_2 Composite Anodes for Lithium Ion Batteries. *J. Mater. Chem. A* **2014**, *2*, 17139−17145.

(30) Zhang, J. J.; Liang, J. W.; Zhu, Y. C.; Wei, D. H.; Fan, L.; Qian, Y. T. Synthesis of Co_2SnO_4 Hollow Cubes Encapsulated in Graphene as High Capacity Anode Materials for Lithium-Ion Batteries. *J. Mater. Chem. A* **2014**, *2*, 2728−2734.

(31) Wang, Z. L.; Xu, D.; Wang, H. G.; Wu, Z.; Zhang, X. B. In Situ Fabrication of Porous Graphene Electrodes for High-Performance Energy Storage. *ACS Nano* **2013**, *7*, 2422−2430.

(32) Zhao, G.; Zhang, N.; Sun, K. Electrochemical Preparation of Porous MoO_3 Film with A High Rate Performance as Anode for Lithium Ion Batteries. *J. Mater. Chem. A* **2013**, *1*, 221−224.

(33) Lin, H. B.; Rong, H. B.; Huang, W. Z.; Liao, Y. H.; Xing, L. D.; Xu, M. Q.; Li, X. P.; Li, W. S. Triple-Shelled Mn_2O_3 Hollow Nanocubes: Force-Induced Synthesis and Excellent Performance as the Anode in Lithium-Ion Batteries. *J. Mater. Chem. A* **2014**, *2*, 14189−14194.

(34) Bai, Z. C.; Fan, N.; Ju, Z. C.; Guo, C. L.; Qian, Y. T.; Tang, B.; Xiong, S. L. Facile Synthesis of Mesoporous Mn_3O_4 Nanotubes and Their Excellent Performance for Lithium-Ion Batteries. *J. Mater. Chem. A* **2013**, *1*, 10985−10990.

(35) Hara, D.; Ikuta, H.; Uchimoto, Y.; Wakihara, M. Electrochemical Properties of Manganese Vanadium Molybdenum Oxide as the Anode for Li Secondary Batteries. *J. Mater. Chem.* **2002**, *12*, 2507−2512.

(36) Hara, D.; Shirakawa, J.; Ikuta, H.; Uchimoto, Y.; Wakihara, M.; Miyanaga, T.; Watanabe, I. Charge/Discharge Reaction Mechanism of Manganese Vanadium Oxide as A High Capacity Anode Material for Lithium Secondary Battery. *J. Mater. Chem.* **2002**, *12*, 3717−3722.

(37) Kim, S. S.; Ogura, S.; Ikuta, H.; Uchimoto, Y.; Wakihara, M. Reaction Mechanisms of $MnMoO_4$ for High Capacity Anode Material of Li Secondary Battery. *Solid State Ionics* **2002**, *146*, 249−256.

(38) Yang, G. Z.; Cui, H.; Yang, G. W.; Wang, C. X. Self-Assembly of $Co_3V_2O_8$ Multi layered Nanosheets: Controllable Synthesis, Excellent Li-Storage Properties, and Investigation of Electrochemical Mechanism. *ACS Nano* **2014**, *8*, 4474−4487.

(39) Meduri, P.; Clark, E.; Kim, J. H.; Dayalan, E.; Sumanasekera, G. U.; Sunkara, M. K. MoO_{3-x} Nanowire Arrays as Stable and High-Capacity Anodes for Lithium Ion Batteries. *Nano Lett.* **2012**, *12*, 1784−1788.

(40) Xiao, L.; Zhao, Y.; Yin, J.; Zhang, L. Clewlike ZnV_2O_4 Hollow Spheres: Nonaqueous Sol-Gel Synthesis, Formation Mechanism, and Lithium Storage Properties. *Chem. - Eur. J.* **2009**, *15*, 9442−9450.

(41) Butt, F. K.; Tahir, M.; Cao, C.; Idrees, F.; Ahmed, R.; Khan, W. S.; Ali, Z.; Mahmood, N.; Tanveer, M.; Mahmood, A.; Aslam, I. Synthesis of Novel ZnV_2O_4 Hierarchical Nanospheres and Their Applications as Electrochemical Supercapacitor and Hydrogen Storage Material. *ACS Appl. Mater. Interfaces* **2014**, *6*, 13635−13641.

(42) Liu, X.; Lyu, Y.; Zhang, Z.; Li, H.; Hu, Y. S.; Wang, Z.; Zhao, Y.; Kuang, Q.; Dong, Y.; Liang, Z.; Fan, Q.; Chen, L. Nanotube Li_2MoO_4: A Novel and High-Capacity Material as A Lithium-Ion Battery Anode. *Nanoscale* **2014**, *6*, 13660−13667.

(43) Cui, J.; Da, D.; Jiang, W. Structure Characterization of Vanadium Oxide Thin Films Prepared by Magnetron Sputtering Methods. *Appl. Surf. Sci.* **1998**, *133*, 225−229.

(44) Bondarenka, V.; Martunas, Z.; Kaciulis, S.; Pandolfi, L. Sol-Gel Synthesis and XPS Characterization of Sodium-Vanadium Oxide Bronze Thin Films. *J. Electron Spectrosc. Relat. Phenom.* **2003**, *131-132*, 99−103.

(45) Fleisch, T. H. An XPS Study of the UV Reduction and Photochromism of MoO_3 and WO_3. *J. Chem. Phys.* **1982**, *76*, 780−786.

(46) Moulde, J. C.; King, R. C. *Handbook of X-ray Photoelectron Spectroscopy: A Reference Book of Standard Spectra for Identification and Interpretation of XPS Data*; Perkin-Elmer: Eden Prairie, MN, 1992.

(47) Kim, S. W.; Lee, H. W.; Muralidharan, P.; Seo, D. H.; Yoon, W. S.; Kim, D. K.; Kang, K. Electrochemical Performance and Ex Situ Analysis of $ZnMn_2O_4$ Nanowires as Anode Materials for Lithium Rechargeable Batteries. *Nano Res.* **2011**, *4*, 505−510.

(48) Sun, Y.; Li, C.; Wang, L.; Wang, Y.; Ma, X.; Ma, P.; Song, M. Ultralong Monoclinic ZnV_2O_6 Nanowires: Their Shape-Controlled Synthesis, New Growth Mechanism, and Highly Reversible Lithium Storage in Lithium-Ion Batteries. *RSC Adv.* **2012**, *2*, 8110−8115.